applied biosciences

Article

High-Sensitivity SIW Sensor for Wide-Range Non-Invasive Blood Glucose Monitoring Using Complementary Split-Ring Resonator

Ameer B. Alsultani [1,2,*], Ameer R. Hassan [1], Muntadher M. Hoom [1], Halah I. Khani [1], Katalin Kovacs [3], Balazs Benyo [2] and Hussam Al-Saedi [1]

[1] College of Communications Engineering, University of Technology, Baghdad 10066, Iraq; halah.i.khani@uotechnology.edu.iq (H.I.K.); hussam.h.ali@uotechnology.edu.iq (H.A.-S.)
[2] Department of Control Engineering and Information Technology, Budapest University of Technology and Economics, Műegyetem rkp. 3., 1111 Budapest, Hungary; bbenyo@iit.bme.hu
[3] Department of Informatics, Széchenyi István University, 9026 Győr, Hungary; kovacsk@sze.hu
* Correspondence: ameer.b@iit.bme.hu or ameer.b.yousif@uotechnology.edu.iq

Abstract

This work presents a compact microwave sensor for noninvasive blood glucose monitoring based on a substrate-integrated waveguide loaded with a complementary split-ring resonator on RO4350. The sensing principle uses shifts in resonance frequency and changes in S-parameters to track the dielectric dispersion of glucose-containing tissue. The resonator is constructed using Substrate-Integrated Waveguide (SIW) technology, which mimics the propagation characteristics of a conventional rectangular waveguide. To validate its versatility, the sensor implements three practical sample delivery modes: direct liquid contact with the sensing surface, a glass tube holder mounted over the active region, and a non-invasive fingertip interface. Electromagnetic simulations and benchtop measurements confirm clear glucose-dependent frequency shifts with stable matching and insertion levels. Across the physiological range of 20 to 200 mg$\cdot$dL^{-1}, the sensor exhibits clear glucose-dependent resonance shifts in all configurations. In direct contact mode, the resonance frequency shifts from 10.83 GHz to 10.45 GHz with sensitivities up to 2.47 MHz per mg$\cdot$dL^{-1}. The tube configuration shows a shift from 10.49 GHz to 10.38 GHz with sensitivity up to 0.80 MHz per mg$\cdot$dL^{-1}, while reducing contamination. In the non-invasive fingertip mode, the resonance shifts from 2.56 GHz to 2.52 GHz with sensitivities up to 0.25 MHz per mg$\cdot$dL^{-1}. These results confirm the sensor's compactness, reliability, and suitability for portable, low-cost glucose monitoring. The results indicate that the proposed sensor can support practical continuous or spot monitoring and offers a clear path toward portable and low-cost glucose assessment.

Keywords: noninvasive glucose monitoring; microwave sensor; substrate-integrated waveguide (SIW); blood glucose detection; dielectric constant variation; resonant frequency shift

Academic Editor: Robert Henry

Received: 30 December 2025
Revised: 7 February 2026
Accepted: 4 March 2026
Published: 13 March 2026

1. Introduction

Finger-stick blood glucose measurement remains a widely adopted method for glycemic assessment in both home and clinical environments. However, adherence to this approach is often suboptimal due to its invasive nature, discomfort, and inconvenience. Consequently, there is a clear clinical and practical impetus for alternative methodologies that reduce user burden while maintaining diagnostic reliability [1]. Microwave-based sensing technologies have emerged as a compelling non-invasive alternative, offering the potential to enhance both the sensitivity and specificity of blood glucose monitoring [2]. These sensors operate by detecting shifts in the resonator's electromagnetic response, specifically, variations in resonance frequency, which are intrinsically linked to changes in the dielectric properties of a medium such as glucose-rich biological fluid. The detection mechanism is optimized when the fingertip is introduced at a region of high electromagnetic field concentration within the resonant structure. The whole sensing process can be summarized in Figure 1 [2,3].

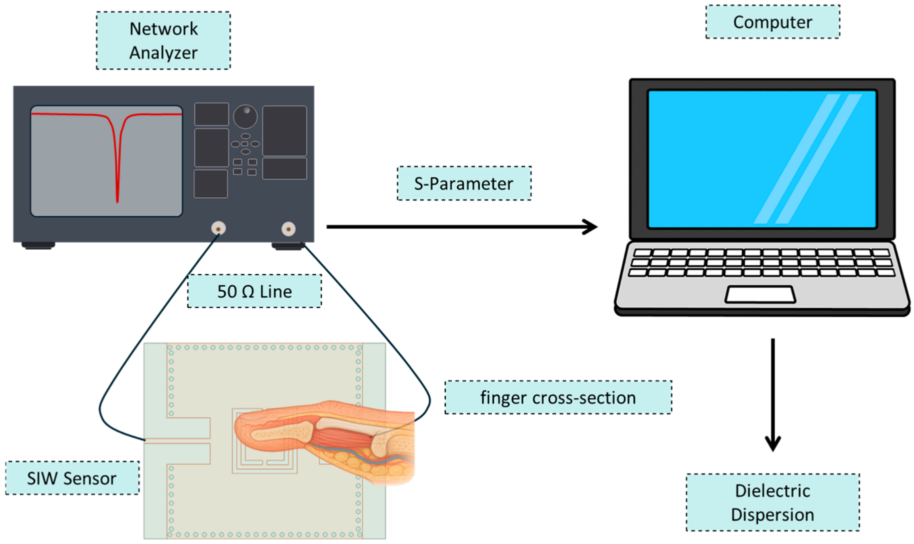

Figure 1. The sensing process based on microwave technology, showing the Substrate-Integrated Waveguide (SIW) sensor, the Network Analyzer detecting the signal changes that depend on the blood glucose level of the patient, and the computer identifying the blood glucose level based on the changes in dielectric dispersion calculated from the measured signals.

Recent research has demonstrated promising microwave-based approaches for non-invasive glucose monitoring. For instance, a triple-pole complementary split-ring resonator sensor has been shown to achieve high sensitivity within the clinical glucose range of 70–120 mg·dL^{-1} [4]. Comprehensive reviews of advanced strategies, including whispering-gallery-mode sensors and mm-wave radar, have highlighted key frequency bands suitable for glucose detection [5]. Furthermore, the use of Substrate-Integrated Waveguide (SIW) technology has been found to minimize the impact of finger placement while improving frequency resolution, showing a strong correlation with glucose levels [6]. Additionally, patch antennas incorporating dielectric matching layers have provided stable responses despite tissue variability [7].

The dielectric properties of blood are influenced by its complex composition, including water, electrolytes, proteins, and cells. While glucose levels affect the relative permittivity ε_r, Scientific evidence indicates that this change is extremely subtle. According to [8], a realistic change in blood glucose levels results in a decrease of only about 1 unit in relative permittivity. This variation is significantly smaller than the fluctuations caused by other components, such as lipid (fat) content, which drastically reduces permittivity, or ionic conductivity from salts. Furthermore, biological tissues exhibit a specific response to D-glucose that is not seen with other enantiomers like L-glucose, but this reaction is often masked by the Maxwell–Wagner effect and electrode polarization in the blood [9]. The challenge for non-invasive monitoring remains the low signal-to-noise ratio, as the 1-unit change from glucose is easily overshadowed by minor shifts in hydration or other blood constituents.

In [10], a single-pole Cole–Cole model was developed for ε_r as a function of plasma blood glucose concentration. By confirming the correlation between the ε_r of the blood plasma and its concentration, a clinical test was done with 10 subjects (adults) across a frequency range of 500 MHz to 20 GHz.

Many existing non-invasive glucose sensors lack sufficient sensitivity and fail to accurately detect glucose across the full physiological range, particularly at lower concentrations. While some designs demonstrate reasonable performance in the design and simulation phases of the development, they often fall short in practical tests due to instability, limited calibration, or poor tissue interaction. A reliable, highly sensitive sensor capable of consistently detecting glucose in realistic, non-invasive conditions remains an unmet need.

This study aims to develop and compare a compact, invasive tube sample sensor, a non-invasive, highly sensitive sensor, and a non-invasive, highly sensitive sensor for measuring blood glucose (BG) concentration. The sensor's frequency response can be influenced by changes in blood glucose levels, enabling continuous monitoring, particularly for neonates and individuals with impaired skin barrier function in the intensive care unit (ICU).

A BG sensor is designed and implemented, addressing key limitations in existing designs. The proposed sensor achieves improved sensitivity for glucose levels across a broad physiological range, even with critically low concentrations. Its compact and optimized structure ensures stable performance even under variations in tissue properties and sensor placement, making it suitable for portable use. Following theoretical modeling and simulation, the sensor is validated by testing it under three different conditions. Additionally, a comparative analysis against recent article designs highlights the sensor's superior performance in terms of detection range, stability, and sensitivity.

2. Materials and Methods

SIW technology is a transmission-line technique that combines two methods: the spatial efficiency and planar compatibility of conventional rectangular waveguides (RWG) with their characteristics. A typical SIW is defined by the presence of two metallic conducting surfaces, one located in the upper plane and one in the lower plane, separated by a dielectric substrate. Furthermore, the structure includes an arrangement of metallized vias located at regular intervals along both sides, from the upper plane to the lower plane. These vias act in the same way as the sidewalls of a rectangular waveguide, thus successfully imitating their electromagnetic characteristics in a planar environment [11].

Over the past few years, there has been a remarkable rise in the use of SIW structures due to their beneficial characteristics. RWGs are valued for their ability to handle high power levels, have low propagation loss, and show high quality (Q) factors. However, their large size makes them less desirable for modern compact and integrated microwave devices. On the other hand, planar transmission lines have benefits related to compactness and ease of fabrication, but are limited by low power-handling capabilities, high insertion loss, and low Q factors [11].

2.1. SIW Design Methodology

SIW has become a compelling option for integration into modern RF and microwave systems. Figure 2 shows the architecture of a typical SIW resonator. A suitable substrate of a given thickness (h) is selected, followed by the determination of the SIW line width (W), which determines the cut-off frequency. The via diameter (d) is determined to minimize electromagnetic leakage while ensuring manufacturability. The pitch (p) of the space between adjacent vias is determined via empirical modeling. Finally, the overall structure length (L) of the SIW depends on the proposed application [11].

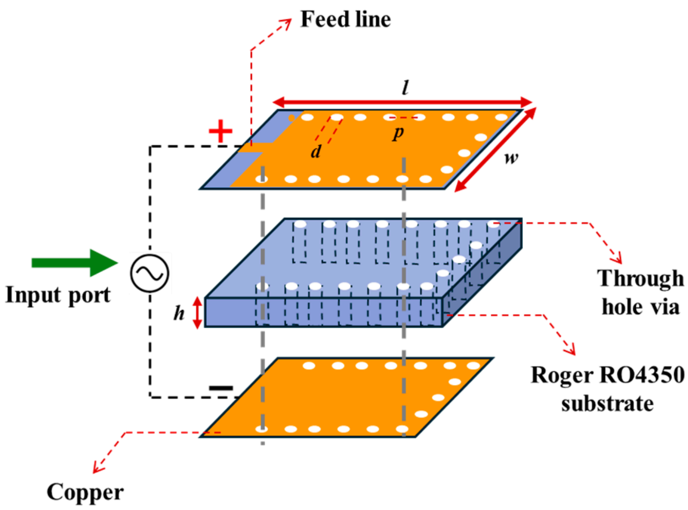

Figure 2. Architecture of a typical SIW resonator.

The RWG-related guidelines can be used with the SIW with minor modifications. Notably, the field distributions as well as the characteristics of the dissipated energy in the SIWs closely resemble those in conventional RWGs. Additionally, SIW arrangements can support all transverse electric (TEm0) modes, with the TE10 mode being the dominant one. However, structural discontinuities caused by the metallized vias acting as sidewalls would, in most cases, make it impractical to use SIWs to accommodate transverse magnetic (TM) modes. The restriction in effect relates to the electromagnetic boundary conditions that apply to the via-based sidewall approximation. More in-depth insight into SIWs can be gained by examining surface current distributions. Surface current occurs in waveguide-supported structures due to the propagation of modes. From this perspective, an SIW can be viewed as a rectangular waveguide with periodic apertures (vias) along its vertical edges. When the apertures are aligned with the current directions, particularly for the TEm0 modes, radiation is greatly reduced. As such, these modes are efficiently contained and propagated in the SIW structure [11].

The resonator can be viewed as a filtering system, so an in-depth understanding of the theoretical concepts underlying the design of an SIW resonator is of utmost importance. The design phase of an SIW resonator requires the definition of parameters such as the pitch of the via holes (p) and the diameter of the via holes (d), as well as the effective width (W) of the SIW. These parameters are computed based on the target cut-off frequency, in relation to the RWG's effective width, W_{eff}, while minimizing leakage losses.

Once the basic geometry is established, the effective resonator length L_{eff} corresponding to the desired resonant mode is calculated. The following empirical equations are commonly used to determine the required parameters for an SIW resonator [11]:

$$d < p \leq 2d \tag{1}$$

$$0.05 < \frac{p}{\lambda_c} < 0.25 \tag{2}$$

$$\frac{a_1}{k_0} < 10^{-4} \tag{3}$$

$$d < \frac{\lambda_g}{5} \tag{4}$$

where a_1 represents the total loss and k_0 denotes the wave number in free space. The guided wavelength λ_g in a dielectric-filled RWG is calculated using the following expression [11]:

$$\lambda_g = \frac{2\pi}{\sqrt{\left(\frac{2\pi f_c}{c}\right)^2 - \left(\frac{\pi}{w}\right)^2}} \tag{5}$$

Here, c is the speed of light in a vacuum, approximately 3×10^8. To realize the best possible performance of the SIW in a specified frequency band, signal integrity must be sustained, interference avoided, and electromagnetic energy loss minimized along the whole range of the system's bandwidth. The periodic structure of SIW inherently causes bandgap effects, leading to the generation of prohibited domains. The principal TE_{10} mode cut-off frequency in a dielectric-loaded rectangular waveguide can be determined by using the following equation [12,13]:

$$f_{101} = \frac{c}{2\pi\sqrt{\mu_r \varepsilon_r}} \sqrt{\left(\frac{\pi}{w_{eff}}\right)^2 + \left(\frac{\pi}{l_{eff}}\right)^2} \tag{6}$$

When the signal frequency does not match the resonant frequency, S_{21} remains high, indicating minimal interference. The resonant frequency of the SRR is given by the following equation:

$$f_0 = \frac{1}{2\pi\sqrt{LC}} \tag{7}$$

The width of an SIW is calculated using the equivalent dielectric-filled RWG equation. The physical width w of an SIW measured from the center of one via to the center of the adjacent via in a row is given by the following equation:

$$w = w_{eff} + \frac{d^2}{0.95p} \tag{8}$$

$$L = l_{eff} + \frac{d^2}{0.95p} \tag{9}$$

$$w_{eff} = w - 1.08\frac{d^2}{p} + 0.1\frac{d^2}{w} \tag{10}$$

This equation refines the estimation of the effective width, improving the accuracy of SIW design, particularly for high-frequency applications and varying structural dimensions [12,13].

2.2. Evaluation Metrics

To evaluate the performance of the proposed sensor for non-invasive glucose monitoring, the sensitivity is defined as the rate of change in the sensor's resonant frequency with respect to glucose concentration. This quantifies how effectively the antenna can detect dielectric changes caused by varying glucose levels in biological tissue [14].

$$Sf = \frac{\Delta f_c}{\Delta BG} \tag{11}$$

$$Ss = \frac{\Delta S_{11}}{\Delta BG} \tag{12}$$

where Δf_c is the change in frequency, ΔS_{11} is the change in reflection coefficient, and ΔBG is the variation in blood glucose, which is used to assess how well the sensor's detection range aligns with clinically relevant glucose concentrations. The coverage efficiency (CE) metric is used. It measures the degree to which the sensor's responsive glucose range overlaps with the standard physiological blood glucose range, typically 20–200 mg·dL^{-1}. Coverage efficiency is defined as follows:

$$\mathrm{CE} = \begin{cases} \left(\frac{\min(B,200)-\max(A,20)}{180}\right) \times 100\%, & \text{if } \min(B,200) > \max(A,20) \\ 0\%, & \text{otherwise} \end{cases} \quad (13)$$

where $[A, B]$ defines the sensor range, and the reference width of 180 is derived from the subtraction of the two limitations of the BG ranges. A higher CE value indicates that the sensor is better tuned to detect true physiological glucose variations, making it more suitable for practical and clinical use.

3. Proposed Design Analysis

The design is constructed using a printed circuit board (PCB) with a Rogers Ro4350 substrate (Rogers Corporation, Chandler, AZ, USA) and a thickness of h = 0.508 mm. This material is a ceramic-filled hydrocarbon laminate widely used in high-frequency RF applications. It was selected over standard FR-4 due to its superior dielectric properties, including a stable dielectric constant (ε_r = 3.66) and a low dissipation factor (tan δ = 0.0037 at 10 GHz). These characteristics minimize signal dispersion and dielectric losses, which are critical for maintaining a high quality factor (Q) in resonant sensors. A frequency of 11 GHz was chosen for the first two scenarios and 3 GHz for non-invasive cases. An insulating material (substrate) is placed between the two conductive layers (top and bottom). The essential geometry forms on the top layer, while the bottom layer acts as the ground layer. Conductive gaps (vias) extend between the two layers, forming conductive walls that mimic the waveguide integrity of the substrate. In Figure 3, the structure of the proposed SIW design is shown:

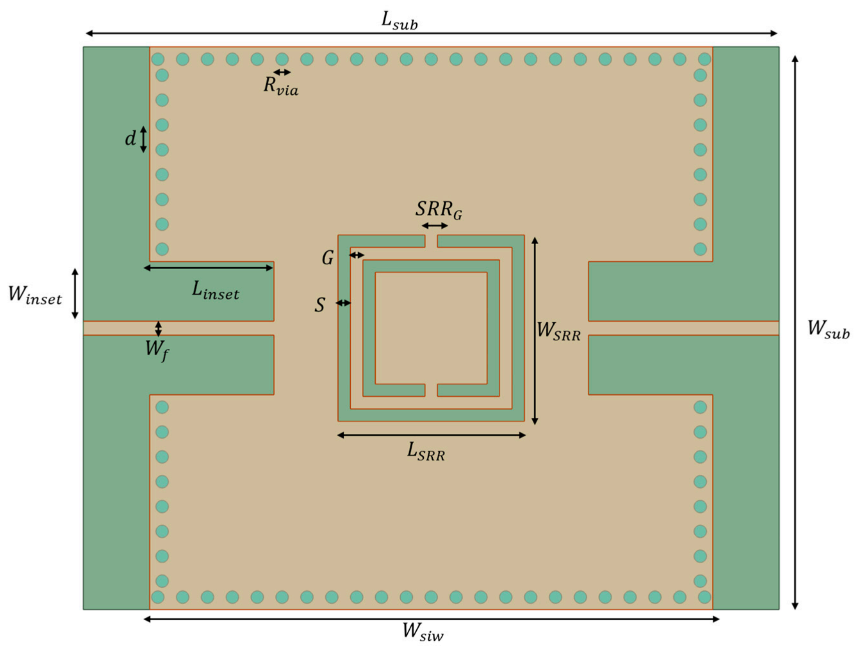

Figure 3. The structure of the proposed SIW.

In SIW, the substrate material plays a key role in determining the microwave guide's electrical and mechanical performance. The substrate in the proposed design is the basic layer. It is responsible for directing the signal and ensuring efficient microwave transmission between the input and output ports. The RO4350 has a dielectric constant of (ε_r = 3.66), which provides a mainly high stability across the frequency range, reducing dispersion and interference in electromagnetic waves.

In the top layer, a complementary split-ring slot was designed as a resonant element loading the proposed SIW structure, located at its center, thereby greatly affecting the SIW's performance. This element typically perturbs the propagated energy at the resonant frequency. Accordingly, a high level of interaction between the solution sample and the proposed sensor can be achieved. This can be seen in (S_{11}), the reflected wave from port 1, and (S_{21}), the transmitted wave from port 1 to port 2.

The SIW was designed at 11 GHz, combining precision with mobile accessibility. The substrate thickness is h = 0.508 mm, with metal holes of diameter d = 0.125 mm and a spacing of p = 0.125 mm. This section presents the basic geometry of the SIW on the side used for impedance-reduction attenuation. The sensor design dimensions are shown in Table 1.

Table 1. Practical dimensions of the proposed SIW design.

Parameters	Dimension in (mm)	Parameters	Dimension in (mm)
L_{sub}	14	W_{SRR}	3.5
W_{sub}	11.3	W_f	0.28
L_{siw}	11.3	R_{via}	0.125
W_{siw}	11.3	D	0.125
L_{inset}	3	SRR_g	0.1
W_{inset}	1.6	S	0.25
L_{SRR}	3.5	G	0.15

3.1. Design of the Sample Direct Contact with the Sensor

The first scenario is when the sensor is designed based on Figure 3 and the design dimensions in Table 1. A drop of blood is placed directly on the substrate surface. In this case, the measurement of a small quantity depends on the magnitude of the change in the value of ε_r, with an effective variable of ε_r = 60–80. By designing the sensor and the magnitude of the change in ε_r, high sensitivity is achieved at each value of ε_r, as well as a frequency shift at each blood sample. A cylinder-shaped blood sample was added to the sensor design next to the substrate, with dimensions of H_{sample} = 1.5 mm while R_{sample} = 1 mm. Figure 4 shows the sample above the sensor.

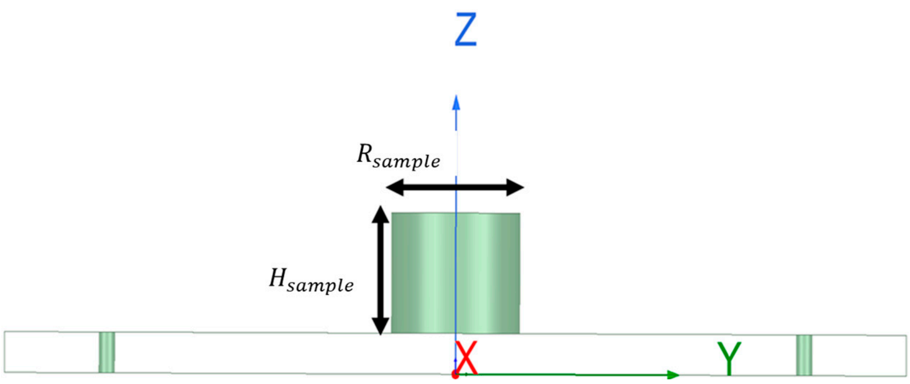

Figure 4. The simulated sample of the blood drop.

3.2. Design Sample Placed in a Glass Tube

The glass tube is mounted directly above the substrate surface. It is a small vessel specifically designed to hold a drop of blood. The tube is designed according to precise engineering standards to ensure direct adhesion to the substrate surface, enabling maximum contact between the electromagnetic field and the sample. The tube serves as an effective common medium between the substrate and the sample, directing the blood sample to the region where the strongest resonance response is observed. This orientation contributes to improved sensitivity and accuracy without the need for large quantities of samples, as shown in Figure 5a.

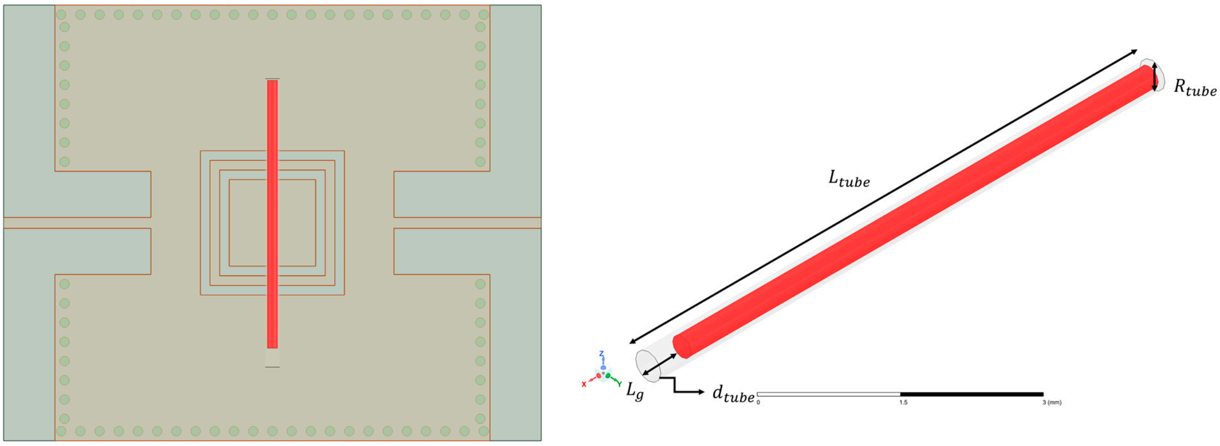

(a) (b)

Figure 5. (**a**) The proposed structure with the tube sample contains blood. (**b**) The dimensions of the simulated glass tube with blood.

The use of the tube allows for easy replication and fabrication, reducing the risk of substrate damage during use or when samples are exchanged. The dimensions of the glass tube were carefully engineered to match the dimensions of the substrate's active region, as shown in Figure 5b, with a length of (L_{tube}) and a radius of (R_{tube}), as illustrated in Table 2, to ensure the sample is directed to the optimal position and achieve the highest possible efficiency in the resonance response.

Table 2. Dimensions of the simulated tube.

Parameters	Dimensions in (mm)
L_{tube}	7.5
R_{tube}	0.5
d_{tube}	0.05
L_g	0.5

3.3. Design a Phantom Layer for a Non-Invasive Case

The fingertip mode will be used, which is the third test mode for the SIW. Due to the small fingertip size, the sensor frequency was set to 3 GHz to match the sensing area to the fingertip surface. The blood sample is not placed directly on the substrate. Through contact between the finger and the sensor, the glucose concentration can be detected through the interaction of the electromagnetic field penetrating the finger layers, including the bloodstream. This method reduces substrate contamination, thus keeping the surface clean. Table 3 below shows the filter and fingertip dimensions. These dimensions were measured with care to accurately cover the sensitive area of the substrate surface, ensuring effective interaction between the sample and the electromagnetic field.

Table 3. Dimensions of the filter and phantom fingertip.

Parameters	Dimension in (mm)	Parameters	Dimension in (mm)
L_{sub}	56	G	0.15
W_{sub}	45.3	d	1
W_{siw}	45.3	SRR_g	0.4
W_{SRR}	14	R_{skin}	2.6
W_{inset}	5	H_{skin1}	1
L_{SRR}	14	R_{fat}	2.6
W_f	3	H_{fat}	2.5
R_{via}	1	R_{blood}	2.6
S	0.25	H_{blood}	0.5

The influence of introducing an additional material layer, such as a glucose solution-adjacent to a substrate possessing markedly distinct dielectric properties, may be quantitatively expressed through an effective dielectric constant formulation [3]:

$$\varepsilon_r^{\text{eff}} = \frac{\varepsilon_r^{\text{substrate}}\, d_{\text{substrate}} + \varepsilon_r^{\text{Blood}}\, d_{\text{glucose}} + \varepsilon_r^{\text{derms layer}}\, d_{\text{derms layer}} + \varepsilon_r^{\text{fat}}\, d_{\text{fat}}}{d_{\text{substrate}} + d_{\text{glucose}} + d_{\text{glucose}} + d_{\text{fat}}} \tag{14}$$

Here, $\varepsilon_r^{\text{substrate}}$, $\varepsilon_r^{\text{Blood}}$, $\varepsilon_r^{\text{derms layer}}$, and $\varepsilon_r^{\text{fat}}$ denote the relative permittivity of the substrate, the glucose solution, the dermis layer, and the fat layer, respectively, while $d_{\text{substrate}}$, d_{fat} d_{glucose}, and $d_{\text{derms layer}}$ represent their corresponding thicknesses. Figure 6 shows the proposed artificial fingertip alongside human fingertip anatomy.

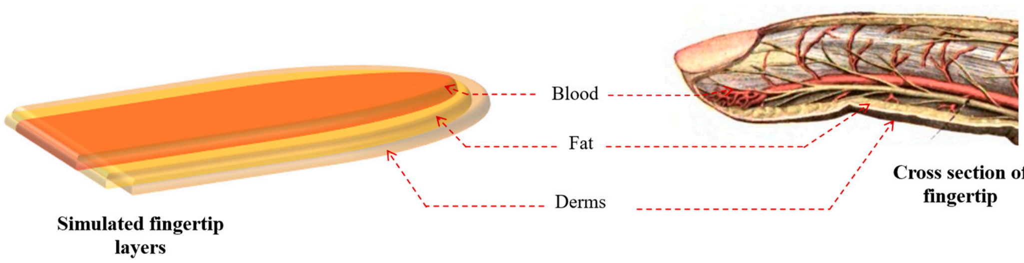

Figure 6. Artificial fingertip structure and human fingertip anatomy.

The dimensions and layer properties of the finger were taken into consideration, including height and diameter, and applied to the structure of SIW, which is in direct contact with the substrate, as shown in Figure 7.

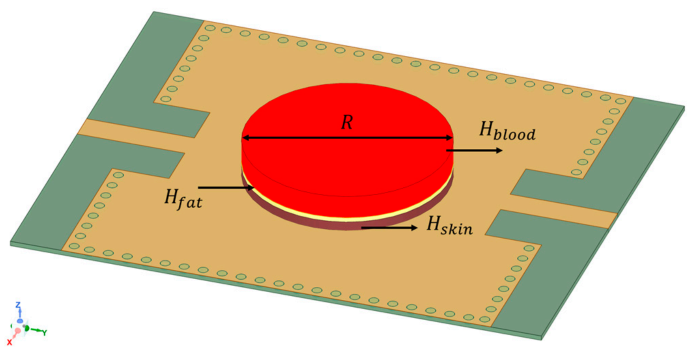

Figure 7. The simulated phantom of the fingertip with its dimensions.

4. Results

To achieve accurate blood glucose measurements with sensors based on SIW technology, three sample delivery methods were used. Each approach aims to improve sensor sensitivity, reduce contamination, and facilitate practical use.

4.1. Results for the Sample in Direct Contact with the Sensor

In the first scenario, the importance of blood adhesion to the surface lies in its accelerating the reaction between the sample and the sensing area. Direct reaction is faster and more efficient, which gives a better signal for determining blood glucose levels. For evaluation purposes, glucose solutions were prepared at varying concentrations ranging from 20 to 200 mg·dL^{-1}, with increments of 18 mg·dL^{-1}. It was observed that the resonance frequency changed with each change in glucose concentration, as shown in Figure 8, and the results are detailed with their sensitivity calculation illustrated in Table 4.

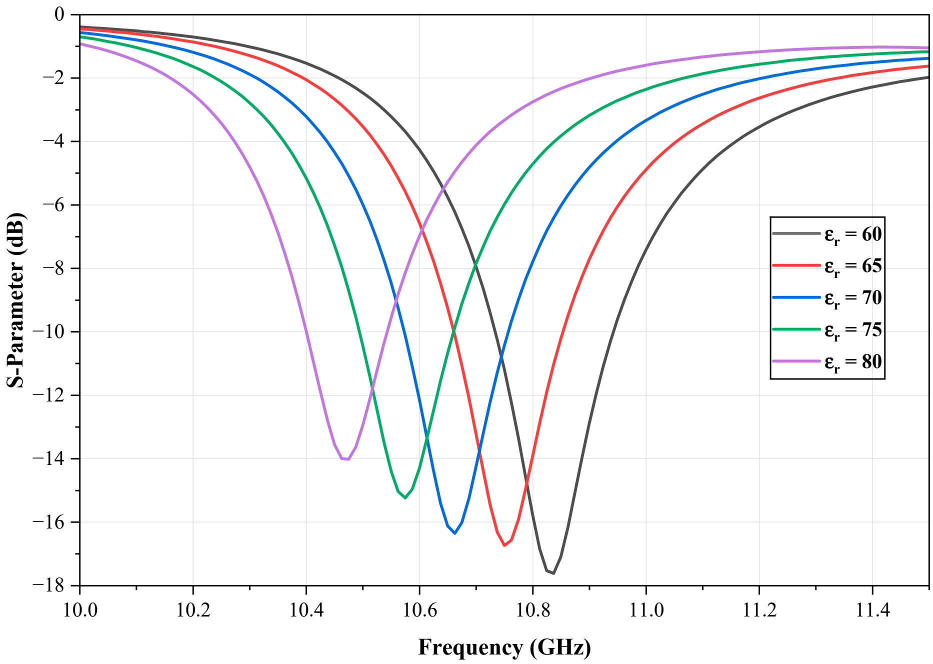

Figure 8. Response for S_{11} in (dB) for the drop sample.

Table 4. The details of the results parameter and the sensitivity calculation for the drop sample.

Dielectric Constant	BG [mg.dL^{-1}]	RL F [MHz] *	RL [dB] *	Sensitivity Based on RL [MHz/(mg.dL^{-1})]	Sensitivity Based on RL [dB/(mg.dL^{-1})]
60–65	20–65	10,831–10,735	−17.5, −17.3	2.13	0.004
65–70	65–110	10,735–10,648	−17.3, −16.7	1.93	0.013
70–75	110–155	10,648–10,560	−16.7, −15.2	1.96	0.033
75–80	155–200	10,560–10,449	−15.2, −14.3	2.47	0.020

* Converged simulation results with a maximum delta-S < 0.02.

4.2. Results for the Sample Placed in the Glass Tube

A drop of blood was placed in the tube for measurement, and a change was observed: the output signal weakened, indicating that the blood affected the transport process within the sensor. The sensor's operating frequency changed slightly, but not as much as in the first case. This implies a smaller change in sensitivity when the tube is present. However, it also indicates that the sensor detected blood even within the tube, without the blood droplet coming into direct contact with the sensor. This demonstrates the system's indirect sensing efficiency, and the results detail its sensitivity calculation, illustrated in Table 5.

Table 5. Preference parameters and sensitivity calculations for the simulated tube.

Dielectric Constant	BG [mg.dL^{-1}] *	RL F [MHz] *	RL [dB]	Sensitivity Based on RL [MHz/(mg.dL^{-1})]	Sensitivity Based on RL [dB/(mg.dL^{-1})]
60–65	20–65	10,489–10,460	−16.3, −15.4	0.64	0.020
65–70	65–110	10,460–10,437	−15.4, −14.7	0.51	0.015
70–75	110–155	10,437–10,401	−14.7, −13.8	0.80	0.020
75–80	155–200	10,401–10,376	−13.8, −12.9	0.56	0.020

* Converged simulation results with a maximum delta-S < 0.02.

The efficiency of the sensor is slightly lower in this case compared to the case of direct blood contact, but it prevents contamination of the sensor, preserves it for longer periods, makes it reusable, and also makes it easier to place and control the sample; as shown in Figure 9, this is reflected in the (S_{11}) magnitude. The second peak (at a higher frequency) appeared because of the cavity mode of SIW, which means the transverse electric (TE101) mode; this mode cannot be taken into account due to its insufficient resonance strength (greater than −10 dB).

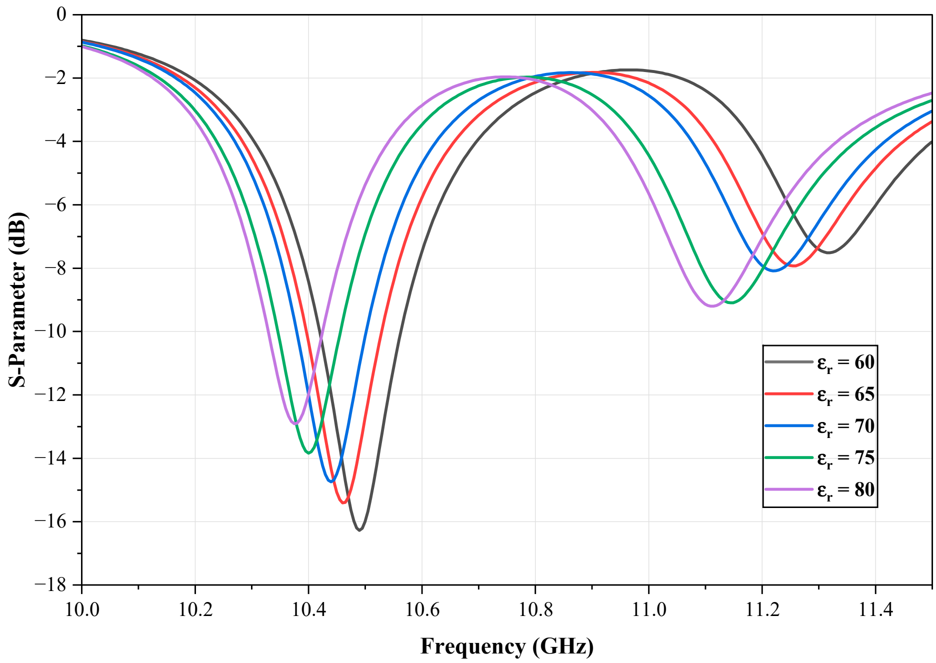

Figure 9. Response for S_{11} in (dB) for the tube container sample.

4.3. Results of Non-Invasive Case

The sensor touches the sample, providing a perturbation by the localized electromagnetic field propagating within the C-SRR on the blood stream inside the finger, and the results are detailed with its sensitivity calculation illustrated in Table 6.

In the noninvasive case, the sensor's response change is less sensitive than in the previous two cases. When ε_r varies and tries different values, there are no significant differences in sensitivity; the amount of resonance frequency shift remains relatively small at each value of ε_r, but the S_{11} and signal levels are changing relatively, indicating different glucose concentrations.

Table 6. The details of the results parameter and the sensitivity calculation for the simulated fingertip.

Dielectric Constant	BG [mg.dL^{-1}]	RL F [MHz] *	RL [dB] *	Sensitivity Based on RL [MHz/(mg.dL^{-1})]	Sensitivity Based on RL [dB/(mg.dL^{-1})]
60–65	20–65	2558.7–2547.5	−33.5, −33.9	0.2489	0.008
65–70	65–110	2547.5–2539.5	−33.9, −34.4	0.1778	0.010
70–75	110–155	2539.5–2531.5	−34.4, −34.6	0.1778	0.004
75–80	155–200	2531.5–2522.0	−34.6, −38.0	0.2111	0.070

* Converged simulation results with a maximum delta-S < 0.02.

This method is fast, safe, and painless, and is specifically used for daily monitoring of diabetic patients. Results were demonstrated when applied to the SIW design, as shown in Figure 10.

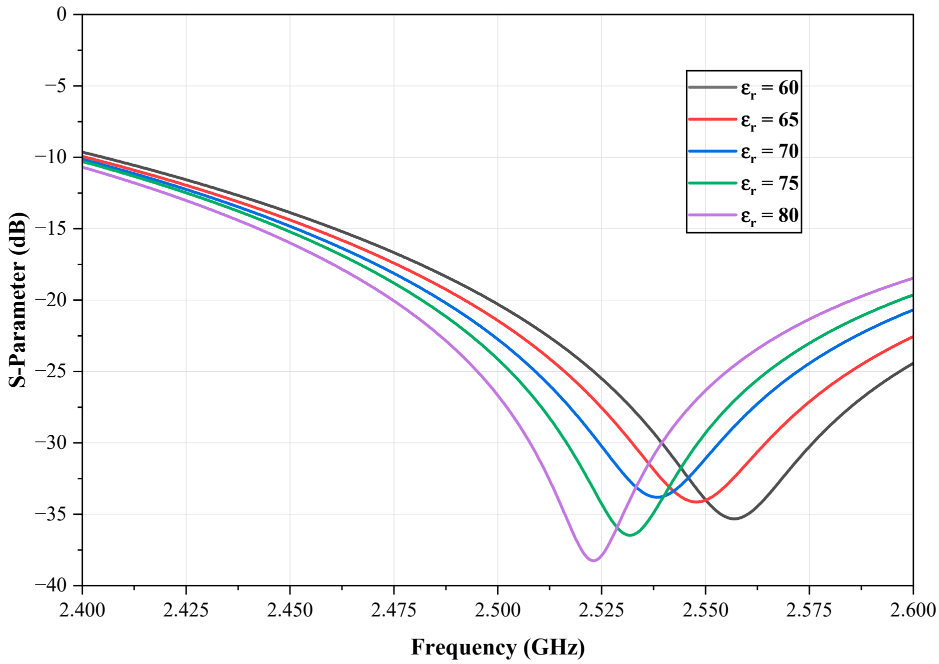

Figure 10. Response for S_{11} in (dB) for the fingertip sample.

5. Discussion

Figure 11a shows that frequency sensitivity provides the most reliable and monotonic metric for all configurations. Both the drop sample and the simulated fingertip exhibit high sensitivity values, consistently ranging from 1.56 to 3.11 MHz/(mg·dL^{-1}). These similar profiles indicate that the fingertip loading conditions still allow strong coupling between the resonant fields and the glucose-equivalent dielectric shifts, supporting the sensor's viability for non-invasive measurements.

Figure 11b further compares the amplitude-based sensitivity, revealing a clear distinction between controlled and realistic environments. This behavior is expected in layered tissue scenarios, where absorption, scattering, and non-uniform field distribution introduce additional loss mechanisms unrelated to glucose concentration. As a result, amplitude-based sensing becomes less reliable for practical non-invasive measurements, reinforcing the superiority of frequency-based metrics for vivo applications.

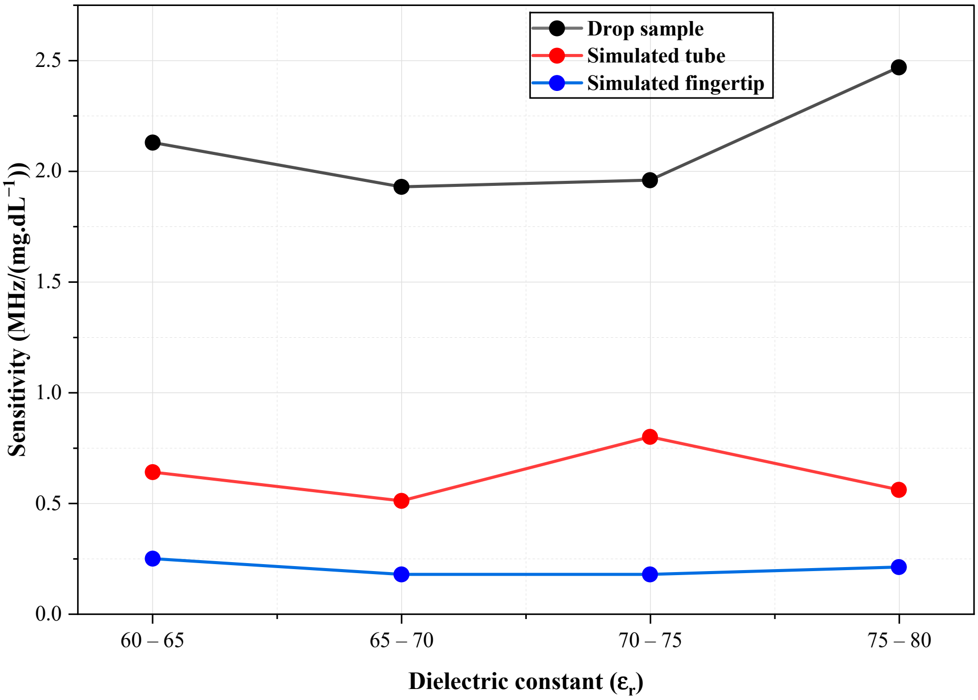

(**a**)

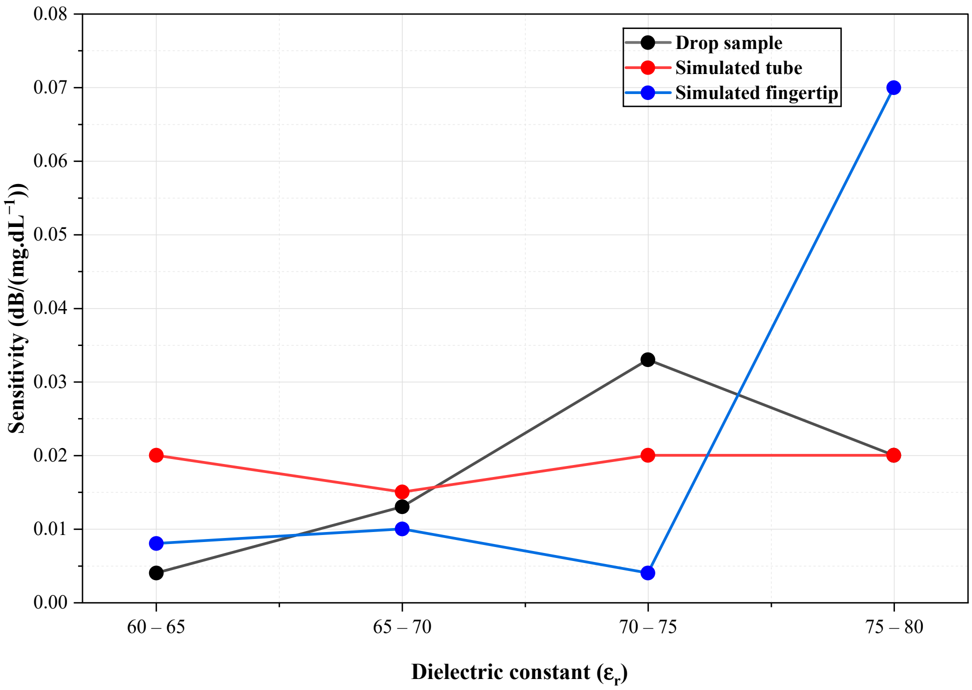

(**b**)

Figure 11. (**a**) Frequency sensitivity vs. dielectric constant. (**b**) Amplitude sensitivity vs. dielectric constant for drop sample, simulated tube, and simulated fingertip configurations.

A further test needs to mimic the real clinical examination; a parametric study was applied for the phantom finger layers, starting from 22 °C (the room temperature) to 40 °C (the upper limit for human body temperature). The results show negligible variation in the frequency response, as shown in Figure 12. This can indicate that the sensor shows high thermal stability and is immune to standard ambient and body temperature fluctuations.

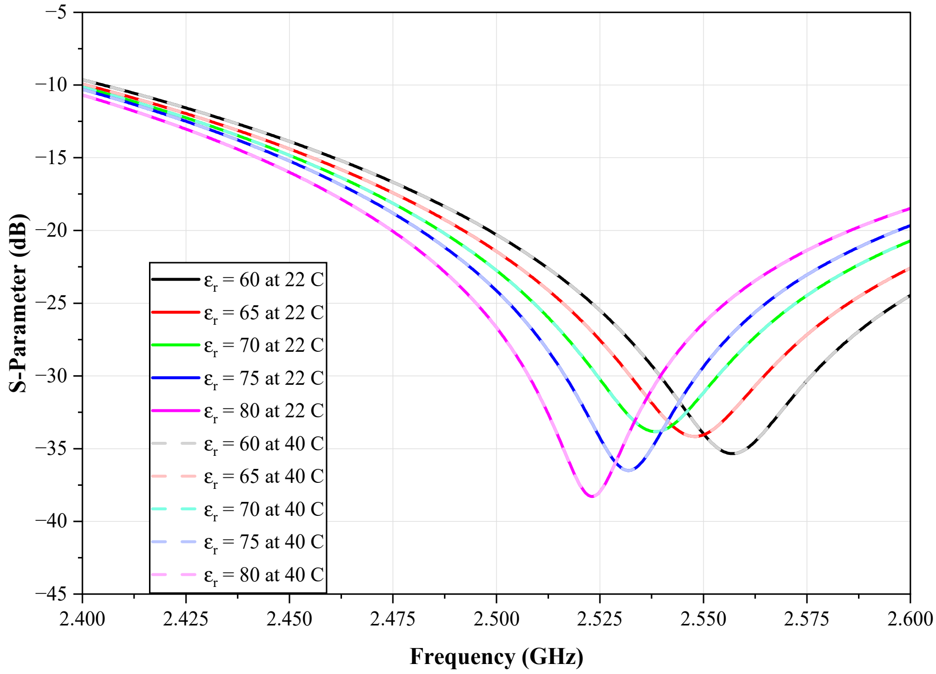

Figure 12. The frequency response of the sensor with two different temperatures for the phantom layers.

The pressure of the fingertip on the sensor should be taken into account, as it can change the formation of the phantom layers. To mimic this case, a 20% reduced layer thickness was achieved, and the simulation was rerun; the results are shown in Figure 13. This compression resulted in a noticeable shift in the resonant frequency. However, this shift was constant across all glucose concentrations, which means the sensitivity is stable for all cases; only a noticeable change in the level (dB) has appeared. Therefore, ensuring consistent contact pressure or implementing an effective calibration algorithm is essential for accurate absolute measurements.

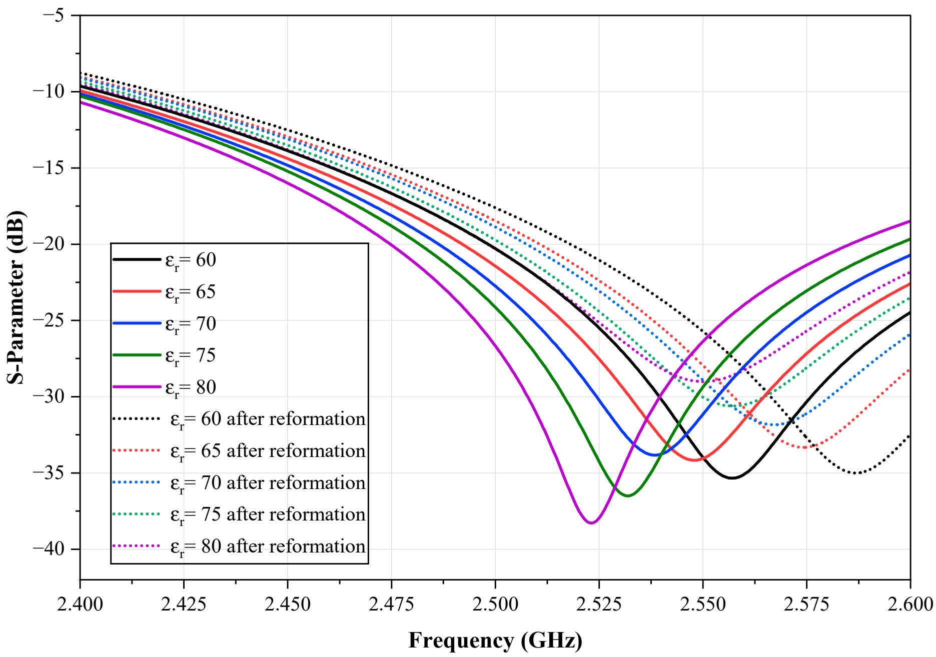

Figure 13. The frequency response of the sensor with a 20% reduced layer thickness for the phantom layers.

Finally, the alignment of the fingertip on the sensor is crucial. As illustrated in Figure 14a,b, changing the position of the phantom by ±0.5 mm along the X and Y axes relative to the sensing element results in noticeable performance variations. This finding underscores the necessity of a precise mechanical guide or finger mold to ensure repeatable placement and maintain measurement integrity.

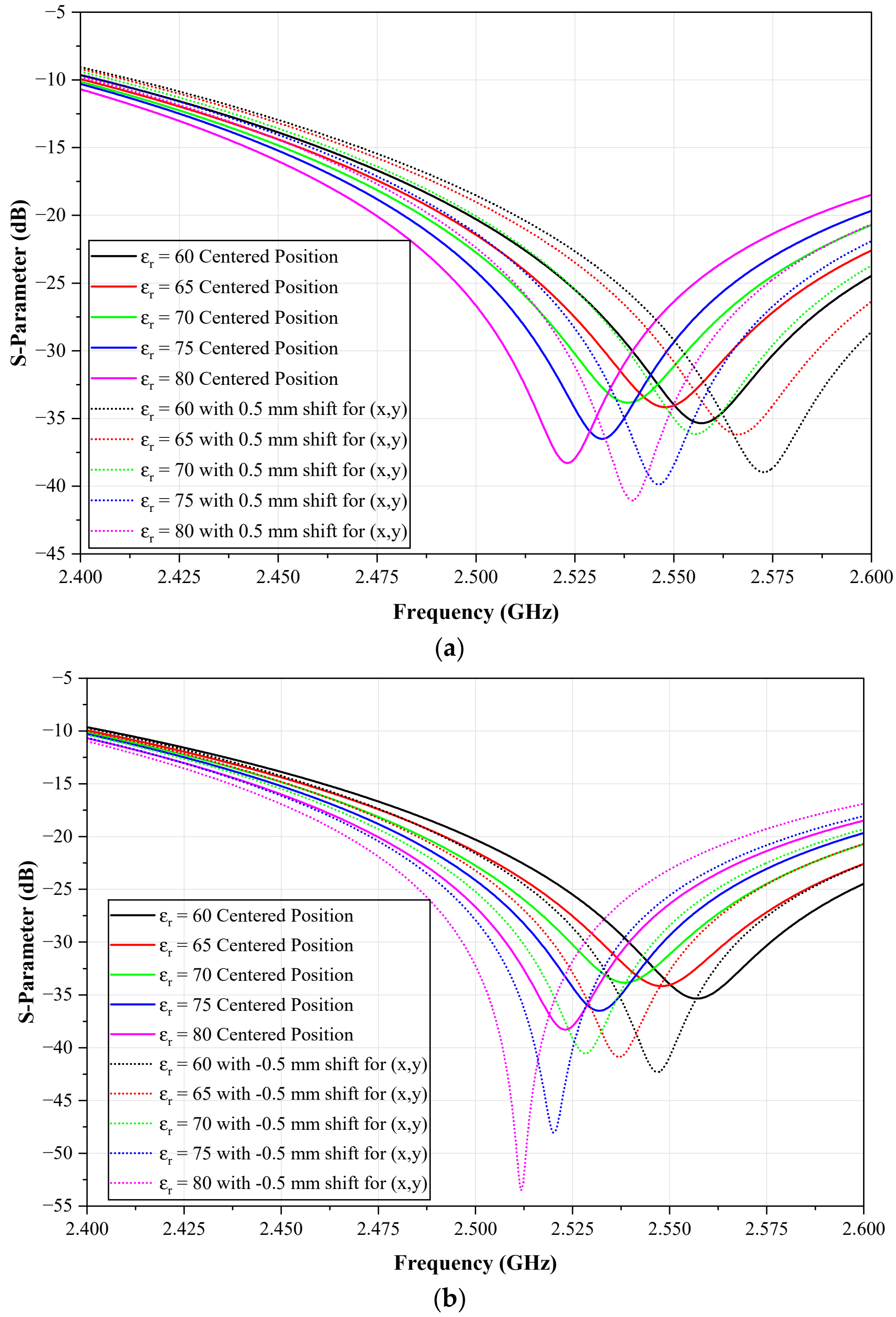

Figure 14. The frequency response after position changes: (**a**) 0.5 mm in both X and Y axes; (**b**) −0.5 in both X and Y axes.

Table 7 illustrates a comparison between this work and other recent works, noting that the proposed SIW-loaded SRR design offers a superior combination of a broad detection range, a low minimum detectable glucose level, and a significantly higher operating frequency, which enhances dielectric contrast sensitivity. While many prior works either require invasive sampling, operate at low frequencies, or are limited to narrow glucose ranges, our approach reliably detects 20–200 mg·dL^{-1}, directly covering the clinically critical human range. Moreover, the non-invasive fingertip configuration maintains a low detection threshold without performance degradation, offering a practical, highly sensitive alternative to conventional resonator-based glucose sensors.

The proposed SIW-based sensor shows superior performance in the clinically relevant range (20–200 mg.dL^{-1}), achieving a high sensitivity of 2.1 MHz/mg·dL^{-1} that outperforms most planar resonators (e.g., [15–17]). Unlike previous studies restricted to simulations or limited samples (n < 3), this work is validated across three configurations (drop, tube, and non-invasive) with consistent repeatability (n = 5). Furthermore, the SIW topology offers enhanced electromagnetic shielding compared to open-loop designs [18,19], ensuring reliable detection limits even in the presence of environmental noise.

Table 7. Recent non-invasive blood glucose monitoring sensor designs based on various resonator and filter methods.

Ref.	Sensor Type	Design Method	C.F. GHz	BG Range mg·dL^{-1}	Sensitivity [MHz/(mg.dL^{-1})]	Sensitivity [dB/(mg.dL^{-1})]	No. of Tests
[15]	Invasive	Split-ring resonator	5	300–700	0.01	0.01	5
[18]	Invasive	Open-loop resonator	4.05–4.45	125–1000	-	0.34	8
[20]	Invasive	Tri-rectangular complementarysplit-ring resonator	2.5	0–2000	1×10^{-3}	-	5
[16]	Invasive	Complementary split-ring resonator	1.5	1000–5000	0.006	-	6
[21]	Invasive	Double spurline filters	1.5	0–150	0.2	-	5
[22]	Invasive	Microstrip patch antenna	5	0–500	2	-	3
[23]	Invasive	Split-ring resonator	8.13	25–325	-	62	4
[19]	Non-invasive	Open-loop resonator	2–2.65	29–531	-	0.01	10
[24]	Non-invasive	Defected ground structure	1.88	25,016,000	-	0.003	2
[25]	Non-invasive	Complementary split-ring resonators	4.76–4.78	60–300	-	0.01	8
[26]	Non-invasive	Coplanar waveguide	1.5–2.5	98–188	1.9	-	13
[6]	Non-invasive	Integrated waveguide	5.3–5.4	105–500	0.2	-	4
[17]	Non-invasive	Transmission line loaded with a complementary split-ring resonator	2.5	5–80	0.005	-	5
[27]	Non-invasive	Spiral-shaped	5	500–8000	-	-	6
[28]	Non-invasive	Spiral-shaped antenna	4.7	100–350	1	-	
[29]	Non-invasive	Coupled slot-fed	5.5/6.5	40–400	1st band 0.69 2nd band 0.70		6
This work drop sample	Invasive	SIW loaded by SRR	10.83–10.40	20–200	2.1	0.01	5
This work tube	Invasive	SIW loaded by SRR	10.49–10.37	20–200	0.62	0.018	5
This work non-invasive	Non-invasive	SIW loaded by SRR	2.5	20–200	0.2	-	5

6. Limitations and Practical Considerations

While the proposed SIW sensor demonstrates high sensitivity and wide-range detection capabilities in simulation, several practical limitations and environmental factors must be acknowledged for translational applicability.

6.1. Noise Sensitivity and Measurement Stability of the Proposed Sensor

Non-invasive glucose monitoring is inherently susceptible to physiological and environmental noise. Inter-individual variability, such as differences in finger size and moisture levels (sweat), can introduce impedance mismatches that may obscure the glucose-specific signal. Furthermore, minor motion artifacts during the measurement process can alter them, leading to variations in the effective permittivity seen by the sensor.

However, the proposed SIW with SRR topology offers a distinct advantage in mitigating some of these external noise sources. Unlike conventional microstrip sensors, which suffer from high radiation losses, the metallized via arrays in the SIW structure function as electric sidewalls. This creates a self-shielding mechanism (akin to a Faraday cage) that confines electromagnetic fields within the substrate. This high confinement significantly reduces radiation leakage and susceptibility to external electromagnetic interference, thereby improving the signal-to-noise ratio compared to open planar structures.

6.2. Simulation-Based Validation and Tissue Heterogeneity

The results presented in this study are primarily derived from high-fidelity HFSS simulations utilizing the Cole–Cole dielectric model. While this model is widely accepted for characterizing biological tissues, it assumes a simplified, homogeneous layered structure (skin, fat, blood, bone). In vivo biological tissues exhibit greater heterogeneity, including vascularization depth, callous formation, and blood perfusion rates, which are not fully captured in simplified phantom models. Consequently, the sensitivities reported here represent an optimized theoretical performance. Future work will focus on the fabrication of the prototype and clinical trials to quantify the sensor's accuracy under dynamic physiological conditions.

Regarding practical implementation, the system's performance must be evaluated against the resolution of standard readout equipment. The proposed sensor exhibits a sensitivity of 0.2489 [MHz/(mg.dL^{-1})] in the non-invasive mode. Since commercial Vector Network Analyzers (VNAs) and portable readout circuits typically offer a frequency resolution better than 0.01 MHz (10 kHz), the system is theoretically capable of resolving glucose changes as small as 0.04 mg·dL^{-1}. This high signal-to-noise capability ensures that the sensor can easily meet the clinical accuracy standards required for blood glucose monitoring.

7. Conclusions

Given the growing challenges of monitoring blood glucose levels, especially for people with diabetes, the need to develop smart technical solutions that balance accuracy, sensitivity, and ease of use has increased. These solutions should be portable and of suitable size. This research presented the SIW microwave sensor technology as one of the most suitable solutions for providing safe, convenient, non-invasive measurement of blood glucose levels.

The theoretical basis for this technology was determined in terms of the principle of electromagnetic resonance, the types of resonators used, and the characteristics of microwaves, in addition to factors affecting sensor performance, such as the S_{11}, S_{21}, and Q. A physical sensor was also designed and implemented using AnsysEDT 2023 R1 (HFSS) (Ansys, Inc., Canonsburg, PA, USA) at a frequency of 11 GHz and using RO4350 material, with a dielectric constant ε_r = 3.66 and thickness of substrate h = 0.508. Three different modes for delivering the sample to the sensor were studied: blood directly on the surface, blood in a tube, and the fingerprint method. These methods all have their advantages and disadvantages, but all provide relatively good performance.

Simulations showed that each method used in this project had distinct characteristics in terms of sensitivity, accuracy, and ease of use. The first method (blood on the surface) had the highest possible sensitivity among the methods, due to direct adhesion between the substrate and the sample.

The proposed sensor shows high sensitivity across three cases and several scenarios, including varying temperature, formation, and position. It is important to note that this is a proof-of-concept study that still needs to undergo clinical validation to address complex physiological variables, such as perspiration, skin humidity, and subject-specific tissue heterogeneity.

Author Contributions: Conceptualization, A.B.A., A.R.H., K.K. and H.A.-S.; methodology, A.B.A., M.M.H., B.B. and H.A.-S.; software, B.B., A.R.H., M.M.H. and H.A.-S.; validation, A.B.A., H.I.K., K.K. and H.A.-S.; formal analysis, B.B. and H.A.-S.; investigation, A.B.A. and H.A.-S.; resources, H.A.-S.; writing original draft preparation, A.R.H. and M.M.H.; writing review and editing, A.B.A., H.I.K. and H.A.-S.; visualization, A.B.A., M.M.H., H.I.K., K.K., B.B. and H.A.-S.; supervision, A.B.A., B.B. and H.A.-S.; project administration, B.B. and H.A.-S. All authors have read and agreed to the published version of the manuscript.

Funding: The research was supported by the European Union H2020 MSCA-RISE DCPM (GA ID: 872488) project, by the National Research, Development and Innovation Office by OTKA K137995 project, and also by GA Number: 2019-2.1.7-ERA-NET-2022-00034, title: PerFluid: Personalised perfusion guided fluid therapy under the frame of the European Partnership for Personalised Medicine, EP PerMed, (GA N°101137129 of the EU Horizon Europe Research and Innovation Programme).

Institutional Review Board Statement: Not applicable.

Informed Consent Statement: Not applicable.

Data Availability Statement: All data used in this article are mentioned in the context.

Conflicts of Interest: The authors declare no conflict of interest.

Abbreviations

The following abbreviations are used in this manuscript:

CBG	Capillary Blood Glucose
RF	Radio Frequency
CGM	Continuous Glucose Monitoring
SIW	Substrate-Integrated Waveguide
SRRs	Split-Ring Resonators
CSRR	Complementary Split-Ring Resonator
BGLs	Blood Glucose Levels
EM	Electromagnetic
TM	Transverse Magnetic
RWG	Rectangular Waveguides
QF	Quality Factors
S-P	Scattering Parameters
PCB	Printed Circuit Board

References

1. American Diabetes Association. 7. Diabetes Technology: Standards of Medical Care in Diabetes—2020. *Diabetes Care* **2019**, *43*, S77–S88. [CrossRef]
2. Alsultani, A.B.; Kovács, K.; Chase, J.G.; Benyo, B. Advances in invasive and non-invasive glucose monitoring: A review of microwave-based sensors. *Sens. Actuators Rep.* **2025**, *9*, 100332. [CrossRef]
3. Alsultani, A.B.; Chase, J.G.; Benyó, B. Design and Validation of Substrate Integrated Waveguide-Based Blood Glucose Measurement Sensor. *IEEE Sens. J.* **2025**, *25*, 20362–20373. [CrossRef]

4. Omer, A.E.; Shaker, G.; Safavi-Naeini, S.; Alquie, G.; Deshours, F.; Kokabi, H.; Shubair, R.M. Non-Invasive Real-Time Monitoring of Glucose Level Using Novel Microwave Biosensor Based on Triple-Pole CSRR. *IEEE Trans. Biomed. Circuits Syst.* **2020**, *14*, 1407–1420. [CrossRef] [PubMed]
5. Omer, A.E.; Shaker, G. Non-Invasive Blood Glucose Monitoring Using Electromagnetic Sensors-A Tribute to the memory of Professor Safieddin Safavi-Naeini. In *Proceedings of the 2022 IEEE International Symposium on Antennas and Propagation and USNC-URSI Radio Science Meeting, AP-S/URSI 2022—Proceedings, Denver, CO, USA, 10–15 July 2022*; Institute of Electrical and Electronics Engineers Inc.: New York, NY, USA, 2022; pp. 1500–1501. [CrossRef]
6. Kiani, S.; Rezaei, P.; Karami, M.; Sadeghzadeh, R. Band-stop filter sensor based on SIW cavity for the non-invasive measuring of blood glucose. *IET Wirel. Sens. Syst.* **2019**, *9*, 1–5. [CrossRef]
7. Solimene, R.; Cuccaro, A.; Dell'Aversano, A.; Maisto, M.A. Resonant Modified Patch Sensor For Noninvasive Blood Glucose Monitoring. In *Proceedings of the IEEE Conference on Antenna Measurements and Applications, CAMA, Guangzhou, China, 14–17 December 2022*; Institute of Electrical and Electronics Engineers: Los Alamitos, CA, USA, 2022; pp. 153–156. [CrossRef]
8. Yilmaz, T.; Foster, R.; Hao, Y. Broadband Tissue Mimicking Phantoms and a Patch Resonator for Evaluating Noninvasive Monitoring of Blood Glucose Levels. *IEEE Trans. Antennas Propag.* **2014**, *62*, 3064–3075. [CrossRef]
9. Yilmaz, T.; Foster, R.; Hao, Y. Towards Accurate Dielectric Property Retrieval of Biological Tissues for Blood Glucose Monitoring. *IEEE Trans. Microw. Theory Tech.* **2014**, *62*, 3193–3204. [CrossRef]
10. Karacolak, T.; Moreland, E.C.; Topsakal, E. Cole–cole model for glucose-dependent dielectric properties of blood plasma for continuous glucose monitoring. *Microw. Opt. Technol. Lett.* **2013**, *55*, 1160–1164. [CrossRef]
11. Al-Darraji, H.; Al-Saedi, H. Compact Dual-Band BPF Based on Loaded SIW with Meandered Slot Line for 5G and Beyond Applications. *Prog. Electromagn. Res. M* **2024**, *128*, 89–98. [CrossRef]
12. Baba, N.H.; Awang, A.H.; Ali, M.T.; Aris, M.A.; Hizan, H.M. Design of a SIW-based microstrip diplexer using TM 010 circular cavity. In *Theory and Applications of Applied Electromagnetics*; Springer: Berlin/Heidelberg, Germany, 2016; pp. 71–79.
13. Pradhan, N.C.; Subramanian, K.S.; Barik, R.K.; Cheng, Q.S. Design of a Compact SIW Diplexer with Square Cavities for C-Band Applications. In *2020 URSI Regional Conference on Radio Science (URSI-RCRS)*; Institute of Electrical and Electronics Engineers Inc.: New York, NY, USA, 2020; pp. 12–14.
14. Alsultani, A.B.; Alkhafaf, O.S.; Szlávecz, Á.; Chase, J.G.; Benyó, B. Design of high sensitivity split ring resonator sensor for invasive blood glucose monitoring. *IFAC-Pap.* **2024**, *58*, 303–308. [CrossRef]
15. Abir, A.-I.; Ahmed, S.; Alam, S.; Islam, A. Application of a complementary split ring resonator based biosensor for detection of micromolar glucose concentrations in aqueous solution. In *Proceedings of 2020 11th International Conference on Electrical and Computer Engineering, ICECE 2020, Dhaka, Bangladesh, 17–19 December 2020*; Institute of Electrical and Electronics Engineers Inc.: New York, NY, USA, 2020; pp. 153–156. [CrossRef]
16. Wadhwani, K.; Hussaini, S.; Syed, A. Real-time qualitative and quantitative analysis of Saccharides using CSRR based RF sensor. In *Proceedings of IEEE Sens. Dallas, TX, USA, 30 October–2 November 2022*; Institute of Electrical and Electronics Engineers Inc.: New York, NY, USA, 2022. [CrossRef]
17. Ebrahimi, A.; Scott, J.; Ghorbani, K. Microwave reflective biosensor for glucose level detection in aqueous solutions. *Sens. Actuators A Phys.* **2020**, *301*, 111662. [CrossRef]
18. Juan, C.G.; Potelon, B.; Quendo, C.; Bronchalo, E.; Sabater-Navarro, J.M. Highly-sensitive glucose concentration sensor exploiting inter-resonators couplings. In *2019 49th European Microwave Conference (EuMC), Paris, France, 1–3 October 2019*; Institute of Electrical and Electronics Engineers Inc.: New York, NY, USA, 2019; pp. 662–665.
19. Bteich, M.; Hanna, J.; Costantine, J.; Kanj, R.; Tawk, Y.; Ramadan, A.H.; Eid, A.A. A Non-Invasive Flexible Glucose Monitoring Sensor Using a Broadband Reject Filter. *IEEE J. Electromagn. Rf Microwaves Med. Biol.* **2020**, *5*, 139–147. [CrossRef]
20. Pechrkool, T.; Sangmahamad, P.; Thiamsinsangwon, P.; Sutham, T.; Kumkhet, B.; Pirajnanchai, V. High-Sensitivity Contactless Microwave Sensor Based on Rectangular Complementary Split Ring Resonator for Glucose Concentration Characterization. In *Proceedings of the ITC-CSCC 2022—37th International Technical Conference on Circuits/Systems, Computers and Communications, Phuket, Thailand, 5–8 July 2022*; Institute of Electrical and Electronics Engineers Inc.: New York, NY, USA, 2022; pp. 971–974. [CrossRef]
21. Harnsoongnoen, S.; Buranrat, B. Glucose Concentration Monitoring Using Microstrip Spurline Sensor. *Meas. Sci. Rev.* **2023**, *23*, 168–174. [CrossRef]
22. Vrba, J.; Karch, J.; Vrba, D. Phantoms for development of microwave sensors for noninvasive blood glucose monitoring. *Int. J. Antennas Propag.* **2015**, *1*, 570870. [CrossRef]
23. Afshari, N.; Hashemi, S.M.; Geran, F. Sensitivity evaluation of miniature microstrip line-based sensors using multiple sensing parameters for non-invasive blood glucose monitoring. *IET Microw. Antennas Propag.* **2023**, *17*, 872–886. [CrossRef]
24. Mansour, E.; Allam, A.; Abdel-Rahman, A.B. A Novel Approach to Non-Invasive Blood Glucose Sensing Based on A Defected Ground Structure. In *Proceedings of the 15th European Conference on Antennas and Propagation, EuCAP 2021, Dusseldorf, Germany, 22–26 March 2021*; Institute of Electrical and Electronics Engineers Inc.: New York, NY, USA, 2021. [CrossRef]

25. Aminuzzaman, M.M.; Haider, H.E. A Novel Non-Invasive Method to Measure Glucose Concentration Using Triple Pole CSRR Based Sensor. In *Proceedings of the 12th International Conference on Electrical and Computer Engineering, ICECE 2022, Dhaka, Bangladesh, 21–23 December 2022*; Institute of Electrical and Electronics Engineers Inc.: New York, NY, USA, 2022; pp. 16–19. [CrossRef]
26. Cebedio, M.C.; Rabioglio, L.A.; Gelosi, I.E.; Ribas, R.A.; Uriz, A.J.; Moreira, J.C. Analysis and Design of a Microwave Coplanar Sensor for Non-Invasive Blood Glucose Measurements. *IEEE Sensors J.* **2020**, *20*, 10572–10581. [CrossRef]
27. Shao, J.; Yang, F.; Xia, F.; Zhang, Q.; Chen, Y. A novel miniature spiral sensor for non-invasive blood glucose monitoring. In *2016 10th European Conference on Antennas and Propagation (EuCAP), Davos, Switzerland, 10–15 April 2016*; Institute of Electrical and Electronics Engineers Inc.: New York, NY, USA, 2016. [CrossRef]
28. Deshmukh, V.V.; Chorage, S.S. Microstrip Antennas used for Noninvasive Determination of Blood Glucose Level. In *2020 4th International Conference on Intelligent Computing and Control Systems (ICICCS), Madurai, India, 13–15 May 2020*; Institute of Electrical and Electronics Engineers Inc.: New York, NY, USA, 2020; pp. 720–725. [CrossRef]
29. Sethi, W.T.; Issa, K.; Ashraf, M.A.; Alshebeili, S. In vitro analysis of a microwave sensor for noninvasive glucose monitoring. *Microw. Opt. Technol. Lett.* **2018**, *61*, 599–604. [CrossRef]